Numer Algor (2018) 79:879–897
https://doi.org/10.1007/s11075-017-0465-z

ORIGINAL PAPER

A numerical algorithm to reduce ill-conditioning in meshless methods for the Helmholtz equation

Pedro R. S. Antunes[1]

Received: 24 May 2017 / Accepted: 26 December 2017 / Published online: 24 January 2018

Abstract Some meshless methods have been applied to the numerical solution of boundary value problems involving the Helmholtz equation. In this work, we focus on the method of fundamental solutions and the plane waves method. It is well known that these methods can be highly accurate assuming smoothness of the domains and the boundary data. However, the matrices involved are often ill-conditioned and the effect of this ill-conditioning may drastically reduce the accuracy. In this work, we propose a numerical algorithm to reduce the ill-conditioning in both methods. The idea is to perform a suitable change of basis. This allows to obtain new basis functions that span exactly the same space as the original meshless method, but are much better conditioned. In the case of circular domains, this technique allows to obtain errors close to machine precision, with condition numbers of order $O(1)$, independently of the number of basis functions in the expansion.

Keywords Method of fundamental solutions · Plane waves · Ill-conditioning · Helmholtz equation

The research was partially supported by FCT, Portugal, through the program "Investigador FCT" with reference If/00177/2013 and the scientific project PTDC/MAT-CAL/4334/2014.

✉ Pedro R. S. Antunes
prantunes@fc.ul.pt

[1] Group of Mathematical Physics, Faculdade de Ciências da Universidade de Lisboa, Campo Grande, Edifício C6, 1749-016 Lisboa, Portugal

1 Introduction

The method of fundamental solutions (MFS) is a numerical method for the solution of boundary value problems with some partial differential equations, provided the fundamental solution of such equations is known. It was introduced in 1964 by Kupradze and Aleksidze [22] and since then it has been widely studied [1, 7, 8, 12, 19, 21, 24]. It is a meshless method that approximates the solution of the boundary value problem by a linear combination of shifts of the fundamental solution to some source points that are located on an auxiliary curve that surrounds the domain.

Under smoothness assumption of the domain and the boundary data, the method may present spectral convergence and it is possible to reach the machine precision with small matrices. In this smooth setting, commonly the accuracy increases once we increase the distance between the auxiliary curve and the boundary of the domain. On the other hand, the matrices involved are dense and often ill-conditioned and this ill-conditioning can reduce the accuracy that can be achieved. This phenomenon, also shared by radial basis functions method, is known in the literature as *uncertainty principle* [27]. Roughly speaking, it states that it is impossible to keep the error and the condition number both small. However, in some sense, this was disproved in [13], where a new numerical algorithm is proposed, the *RBF-QR*, which reveals that the ill-conditioning can be completely removed.

The location of the source points is one of the main issues when applying the MFS. In [7], the authors discussed how the location of these source points can affect the accuracy of the method, taking into account the behavior of the magnitude of the linear combination coefficients. In particular, they concluded that the stability and high accuracy of the method rely on a choice of an auxiliary curve that does not enclose any singularity of the analytic continuation of the solution.

Another meshless method that was already considered for the solution of boundary value problems with Helmholtz equation is the plane waves method (PWM) [4, 9, 11]. In this case, the solution is approximated by a linear combination of plane waves. Taking into account the asymptotic behavior of the fundamental solution, we conclude that this method can be seen as an *asymptotic MFS*, when the source points are placed *far* from the boundary of the domain [4].

Some other methods have been applied for the numerical solution of these kinds of problems, such as the plane wave partition of unity finite element method [6], the ultra weak variational formulation [10], the plane wave discontinuous Galerkin method [14, 15], or the plane wave least-squares method [17, 25]. In these methods, the domain is discretized into a mesh. Then, in each of the elements of the mesh, the solution is approximated by a linear combination of particular solutions of the Helmholtz equation, such as plane waves or Bessel functions. This procedure allows to control the conditioning of the linear system that is obtained.

In this work, we consider the numerical solution of boundary value problems for the Helmholtz equation in planar regions and adapt the main idea of the RBF-QR to reduce the ill-conditioning of the MFS and the PWM. This allows to propose an algorithm that applies a change of basis to the classical MFS and PWM basis functions. The new functions span the same space as the original method, but are much better conditioned. In the case of circular domains, the algorithm allows to obtain errors

close to machine precision, with condition numbers of order $O(1)$, independently of the number of basis functions.

2 The direct approach of the method of fundamental solutions

Let Ω be a smooth bounded planar domain. We consider the following boundary value problem,

$$\begin{cases} \Delta u + \kappa^2 u = 0 & \text{in } \Omega, \\ u = g & \text{on } \partial\Omega, \end{cases} \tag{2.1}$$

for some given function g defined on $\partial\Omega$.

We will denote by Φ_κ a fundamental solution of the Helmholtz equation,

$$\Phi_\kappa(x) = \frac{i}{4} H_0^{(1)}(\kappa|x|),$$

where $H_0^{(1)}$ is a Hankel function of the first kind of order zero. This fundamental solution is analytic, except at the origin, where it has a logarithmic-type singularity. The standard approach of the method of fundamental solutions, which will be called *Direct-MFS*, approximates the solution of the boundary value problem (2.1) by a linear combination

$$u_N^{MFS-Dir}(x) = \sum_{j=1}^{N} \alpha_j^{MFS-Dir} \Phi_\kappa(x - y_j). \tag{2.2}$$

Each base function is a translation of the fundamental solution to some source point y_j placed on some admissible source set $\hat{\Gamma}$ that does not intersect $\bar{\Omega}$. Thus, by construction, it satisfies the PDE of the problem. The approximation of the boundary condition can be justified by density results,

$$span\left\{\Phi_\kappa(\bullet - y)|_\Omega : y \in \hat{\Gamma}\right\}$$

is dense in $\mathcal{H}_\kappa = \left\{v \in H^1(\Omega) : (\Delta + \kappa^2)v = 0\right\}$, with the H^1 topology (e.g., [3]).

The location of the source points motivated a lot of studies (e.g., [1–3, 7, 16]). We will use the notation

$$R_\Omega := \max_{x\in\partial\Omega} \|x\|, \quad r_\Omega := \min_{x\in\partial\Omega} \|x\|$$

and will assume that the source points are distributed uniformly on a circumference of radius $R > R_\Omega$,

$$y_j = R\left(\cos(\gamma_j), \sin(\gamma_j)\right), \ j = 1, ..., N, \quad \gamma_j = \frac{2\pi j}{N}. \tag{2.3}$$

The coefficients of the linear combination (2.2) can be determined by collocation, forcing the boundary conditions of the problem. We consider P collocation points x_i, $i = 1, 2, ..., P$, and solve

$$\mathbf{A}^{MFS-Dir}\boldsymbol{\alpha}^{MFS-Dir} = \mathbf{G}, \tag{2.4}$$

where

$$\mathbf{A}^{MFS-Dir} = \left[\Phi_\kappa(x_i - y_j)\right]_{P\times N}, \quad \mathbf{G} = [g(x_i)]_{P\times 1}$$

and $\boldsymbol{\alpha}^{MFS-Dir}$ is a vector with all the coefficients of the *Direct-MFS* linear combination (2.2). In this work, we took $P = 2N$ and solved (2.4) in the least-squares sense.

The *Direct-MFS* can be highly accurate, even with a small number of source points. For example, the method can achieve exponential convergence on analytic domains and boundary data ([7, 19–21]). On the other hand, the linear least-squares problem is often ill-conditioned, which affects the accuracy and prevents the exponential convergence to be observed in the numerical simulations. In the following section, we will describe a different approach that reduces the problem of ill-conditioning of the *Direct-MFS*, which was already applied to boundary value problems with Laplace equation in [5].

3 A new formulation—the MFS-QR algorithm

We assume that the source points are given by (2.3), for $R > R_\Omega$. Dropping the constant $i/4$ that may be incorporated in the coefficients of the linear combination, by Graf's addition theorem ([11]), each MFS base function can be written as

$$H_0^{(1)}(\kappa|x-y_j|) = H_0^{(1)}(\kappa|y_j|)J_0(\kappa|x|)+2\sum_{n=1}^{\infty} H_n^{(1)}(\kappa|y_j|)J_n(\kappa|x|)\cos(n\beta), \quad (3.1)$$

where β denotes the angle between x and y_j. We will use the notation $\hat{x} = x/|x|$ and $\hat{y}_j = y_j/|y_j|$ and write $\hat{x} = (\cos(\theta), \sin(\theta))$, for some $\theta \in [0, 2\pi)$. Then,

$$\hat{x}.\hat{y}_j = \cos(\theta)\cos(\gamma_j) + \sin(\theta)\sin(\gamma_j) = \cos(\theta - \gamma_j)$$

and by the law of cosines,

$$\hat{x}.\hat{y}_j = |\hat{x}||\hat{y}_j|\cos(\beta) = \cos(\beta).$$

Therefore, writing (3.1) in polar coordinates, we have

$$\psi_j(r,\theta) := H_0^{(1)}(\kappa R)J_0(\kappa r)+$$

$$2\sum_{n=1}^{\infty} H_n^{(1)}(\kappa R)J_n(\kappa r)\left(\cos(n\theta)\cos(n\gamma_j) + \sin(n\theta)\sin(n\gamma_j)\right).$$

Now, it is convenient to define, for each n, the quantities $J^*_{n,\kappa}$ and R^*_n defined through

$$R^*_n = \text{argmax}_{r\in[r_\Omega, R_\Omega]}|J_n(\kappa r)|, \quad J^*_{n,\kappa} = J_n(\kappa R^*_n)$$

and

$$c_n = \begin{cases} H_0^{(1)}(\kappa R)J^*_{0,\kappa} & n = 0 \\ 2H_n^{(1)}(\kappa R)J^*_{n,\kappa} & n > 0. \end{cases} \quad (3.2)$$

In our algorithm, the approximations for $J^*_{n,\kappa}$ were obtained simply by evaluating $|J_n(\kappa r_i)|$, for 10000 equally spaced points $r_i \in [r_\Omega, R_\Omega]$ and taking the maximum among the values that were obtained. This task is very cheap in terms of computational cost and the cost does not depend much on κ.

The MFS basis functions are given by

$$\begin{bmatrix} \psi_1(r,\theta) \\ \psi_2(r,\theta) \\ \vdots \\ \psi_N(r,\theta) \end{bmatrix} = \begin{bmatrix} 1 & \cos(\alpha_1) & \sin(\alpha_1) & \cos(2\alpha_1) & \sin(2\alpha_1) & \cos(3\alpha_1) & \sin(3\alpha_1) & \dots \\ 1 & \cos(\alpha_2) & \sin(\alpha_2) & \cos(2\alpha_2) & \sin(2\alpha_2) & \cos(3\alpha_2) & \sin(3\alpha_2) & \dots \\ \vdots & \vdots & \vdots & \vdots & \vdots & \vdots & \vdots & \ddots \\ 1 & \cos(\alpha_N) & \sin(\alpha_N) & \cos(2\alpha_N) & \sin(2\alpha_N) & \cos(3\alpha_N) & \sin(3\alpha_N) & \dots \end{bmatrix}$$

$$\begin{bmatrix} c_0 & & & & & & & \\ & c_1 & & & & & & \\ & & c_1 & & & & & \\ & & & c_2 & & & & \\ & & & & c_2 & & & \\ & & & & & c_3 & & \\ & & & & & & c_3 & \\ & & & & & & & \ddots \end{bmatrix} \begin{bmatrix} J_0(\kappa r)/J^*_{0,\kappa} \\ J_1(\kappa r)/J^*_{1,\kappa}\cos(\theta) \\ J_1(\kappa r)/J^*_{1,\kappa}\sin(\theta) \\ J_2(\kappa r)/J^*_{2,\kappa}\cos(2\theta) \\ J_2(\kappa r)/J^*_{2,\kappa}\sin(2\theta) \\ J_3(\kappa r)/J^*_{3,\kappa}\cos(3\theta) \\ J_3(\kappa r)/J^*_{3,\kappa}\sin(3\theta) \\ \vdots \end{bmatrix}. \tag{3.3}$$

After truncating this expansion for some $M \in \mathbb{N}$ (such that $2M+1 > N$) the (3.3) can be written as

$$\Theta(r,\theta) = \mathbf{B}\,\mathbf{D}\,\mathbf{F}(r,\theta). \tag{3.4}$$

Note that the matrix $\mathbf{B}$ is well-conditioned, even for large values of N, see for example Lemma 3.3 of [14], and the condition number is equal to $\sqrt{2}$, independently of N. The ill-conditioning of the *Direct-MFS* arises essentially from the diagonal matrix $\mathbf{D}$. To reduce this ill-conditioning, we adapt the construction of the RBF-QR [13] which allows to construct new basis functions. The main idea is to use the fact that if we multiply an invertible matrix from the left in (3.4), this procedure will change the basis functions without modifying the functional space that is generated by them. Thus, we try to find such a suitable matrix to be multiplied from the left.

We start by calculating a QR factorization of the matrix $\mathbf{B}$,

$$\mathbf{B} = \mathbf{Q}\,\mathbf{R},$$

where $\mathbf{Q}$ is unitary and $\mathbf{R}$ is upper triangular. Therefore, we have

$$\Theta(r,\theta) = \underbrace{\mathbf{Q}\,\mathbf{R}}_{\mathbf{B}}\,\mathbf{D}\,\mathbf{F}(r,\theta).$$

The new basis functions are calculated by multiplying from the left the matrix $\mathbf{D_1}^{-1}\,\mathbf{Q}^T$, where $\mathbf{D_1}$ is the first $N \times N$ block of the matrix $\mathbf{D}$. Thus, since $\mathbf{Q}$ is unitary, we have $\mathbf{Q}^T\,\mathbf{Q} = \mathbf{I}$ which implies that

$$\Psi(r,\theta) = \mathbf{D_1}^{-1}\,\mathbf{Q}^T\,\mathbf{Q}\,\mathbf{R}\,\mathbf{D}\,\mathbf{F}(r,\theta) = \mathbf{D_1}^{-1}\,\mathbf{R}\,\mathbf{D}\,\mathbf{F}(r,\theta).$$

The product $\mathbf{D_1}^{-1}\,\mathbf{R}\,\mathbf{D}$ must be calculated carefully, in order to avoid floating point underflow and/or overflow. The matrix $\mathbf{R}$ is upper triangular and $\mathbf{D}$ and $\mathbf{D_1}$ are diagonal. Thus,

$$\mathbf{D_1}^{-1}\,\mathbf{R}\,\mathbf{D} = \mathbf{T_L} \circ \mathbf{R} \circ \mathbf{T_R}, \tag{3.5}$$

where $\circ$ denotes the Hadamard product of matrices,

$$(\mathbf{A} \circ \mathbf{B})_{i,j} = (\mathbf{A})_{i,j}.(\mathbf{B})_{i,j},$$

and the matrices $\mathbf{T}_R$ and $\mathbf{T_L}$ are defined by

$$\mathbf{T}_R = \begin{bmatrix} c_0 & c_1 & c_1 & c_2 & c_2 & \dots & c_M & c_M \\ & c_1 & c_1 & c_2 & c_2 & \dots & c_M & c_M \\ & & c_1 & c_2 & c_2 & \dots & c_M & c_M \\ & & & c_2 & c_2 & \dots & c_M & c_M \\ & & & & c_2 & \dots & c_M & c_M \\ & & & & & \ddots & & \ddots \end{bmatrix}_{N\times(2M+1)}$$

and

$$\mathbf{T_L} = \begin{bmatrix} 1/c_0 & 1/c_0 & 1/c_0 & 1/c_0 & 1/c_0 & \dots & 1/c_0 & 1/c_0 \\ & 1/c_1 & 1/c_1 & 1/c_1 & 1/c_1 & \dots & 1/c_1 & 1/c_1 \\ & & 1/c_1 & 1/c_1 & 1/c_1 & \dots & 1/c_1 & 1/c_1 \\ & & & 1/c_2 & 1/c_2 & \dots & 1/c_2 & 1/c_2 \\ & & & & 1/c_2 & \dots & 1/c_2 & 1/c_2 \\ & & & & & \ddots & & \ddots \end{bmatrix}_{N\times(2M+1)}.$$

Now we note that the Hadamard product is commutative, which implies that

$$\mathbf{D_1}^{-1}\,\mathbf{R}\,\mathbf{D} = \mathbf{T_L} \circ \mathbf{R} \circ \mathbf{T_R} = \mathbf{T_L} \circ \mathbf{T_R} \circ \mathbf{R} = \tilde{\mathbf{T}} \circ \mathbf{R} := \tilde{\mathbf{R}}, \tag{3.6}$$

where

$$\tilde{\mathbf{T}} = \begin{bmatrix} 1 & c_1/c_0 & c_1/c_0 & c_2/c_0 & c_2/c_0 & \dots & c_M/c_0 & c_M/c_0 \\ & 1 & 1 & c_2/c_1 & c_2/c_1 & \dots & c_M/c_1 & c_M/c_1 \\ & & 1 & c_2/c_1 & c_2/c_1 & \dots & c_M/c_1 & c_M/c_1 \\ & & & 1 & 1 & \dots & c_M/c_2 & c_M/c_2 \\ & & & & 1 & \dots & c_M/c_2 & c_M/c_2 \\ & & & & & \ddots & & \ddots \end{bmatrix}_{N\times(2M+1)}.$$

The new basis functions are defined by the N entries of the vector

$$\Psi(r,\theta) = \mathbf{D_1}^{-1}\,\mathbf{R}\,\mathbf{D}\,\mathbf{F}(r,\theta) = \tilde{\mathbf{R}}\mathbf{F}(r,\theta)$$

and the *MFS-QR* approximation is given in polar coordinates by the linear combination

$$u_N^{MFS-QR}(r,\theta) = \sum_{n=1}^{N} \alpha_n^{MFS-QR}\Psi_n(r,\theta). \tag{3.7}$$

Remark 1 Our algorithm is based on the expansion (3.4), which depends on the choice of the parameter M. This parameter is chosen iteratively, in a such a way that the terms of the matrices $\tilde{\mathbf{R}}$ are small enough. In praxis, we start choosing $M = 2N + 1$ and then increase M until all the components of the Mth column of $\tilde{\mathbf{R}}$ are smaller than machine precision. A good improvement of the algorithm would be to derive bounds for the components of the matrix $\tilde{\mathbf{R}}$ which would allow to choose a convenient value of M, avoiding the iterative procedure that was considered in this paper.

The calculation of the matrix $\tilde{\mathbf{T}}$ shall be performed in a convenient way to avoid underflow/overflow problems. In this context, some asymptotic expansions for the Bessel functions can be used. For example, we have [26]

$$J_m(z) \sim \frac{1}{\sqrt{2\pi m}} \left(\frac{ez}{2m}\right)^m, \quad m \to \infty$$

and

$$Y_m(z) \sim -\sqrt{\frac{2}{\pi m}} \left(\frac{ez}{2m}\right)^{-m}, \quad m \to \infty.$$

In practice, the construction of the matrix $\tilde{\mathbf{T}}$ involves the calculation of ratios of type c_P/c_Q, for $P > Q$, but for large values of Q, we will have underflow problems and the program will give $c_Q = 0$. In that case, the calculation of the ratio c_P/c_Q is replaced by the quantity obtained from the previous two asymptotic formulas.

The MFS-QR procedure is summarized in Algorithm 1.

Algorithm 1 Algorithm of the MFS-QR method

1: Choose N and R.
2: Choose $M = 2N$.
3: Compute $J^*_{n,\kappa}$ and c_n, $n = 0, 1, ..., M$.
4: **Repeat**
5: $M \to M + 1$.
6: Compute the QR factorization of the matrix $\mathbf{B}$.
7: Compute $J^*_{M,\kappa}$ and c_M.
8: Compute $\tilde{\mathbf{R}}$.
9: **Until** all the components Mth column of $\tilde{\mathbf{R}}$ are smaller then machine precision
10: Evaluate $\mathbf{F}(r, \theta)$ at the desired points and multiply against $\tilde{\mathbf{R}}$.

Again, the coefficients of the linear combination can be determined imposing the boundary conditions of the boundary value problem, by solving the linear least-squares problem

$$\mathbf{A}^{MFS-QR}\, \boldsymbol{\alpha}^{MFS-QR} = \mathbf{G}, \tag{3.8}$$

where $\mathbf{A}^{MFS-QR} = [\Psi(x_i)]^T$ or equivalently

$$[\mathbf{F}(x_i)]^T\ \tilde{\mathbf{R}}^T\, \boldsymbol{\alpha}^{MFS-QR} = \mathbf{G}.$$

By construction, the *MFS-QR* approximation is a particular solution of the Helmholtz equation, because the components of $\mathbf{F}(r, \theta)$ also satisfy the equation.

The quality of the approximation $\tilde{u}$ obtained from the *Direct-MFS* or from the *MFS-QR* can be checked *a posteriori* by measuring the L^2 norm of the error on the boundary. As proved in [23], if κ^2 is not a Dirichlet eigenvalue of the Laplacian, then we have the following bound for the error

$$\|u - \tilde{u}\|_{L^2(\Omega)} \leq \frac{C}{d} \|u - \tilde{u}\|_{L^2(\partial\Omega)} = \frac{C}{d} \|g - \tilde{u}\|_{L^2(\partial\Omega)}, \tag{3.9}$$

where C is a constant that depends just on the domain, $d := min_j|\kappa^2 - \lambda_j|/\lambda_j$, and λ_j are the Dirichlet-Laplacian eigenvalues of Ω.

4 The MPW-QR algorithm

Another Treffz-type method is the plane waves method (PWM). In this case, for given unitary directions $d_1, d_2, ..., d_N$, the numerical approximation for the solution of the boundary value problem is a linear combination of plane waves,

$$u_N^{PWM-Dir}(x) = \sum_{j=1}^{N} \alpha_j^{PW-Dir} e^{i\kappa x.d_j}. \tag{4.1}$$

As discussed in [4], taking into account the asymptotic properties of the fundamental solution, the PWM may be seen as a limit case of the MFS with source points located on a circumference with large radius.

The approximation of the boundary condition is justified by a density result, stating that if Ω is a bounded simply connected domain and κ is not an eigenfrequency of Ω, then (e.g., [11])

$$L^2(\partial\Omega) = \overline{\text{span}\left\{e^{i\kappa x.d} : d \in S^1\right\}}.$$

It is straightforward to apply the ideas of the $MFS-QR$ in the context of the plane waves method and we will call to this new approach $PWM-QR$. By Jacobi-Anger expansion ([11]), we have

$$e^{i\kappa x.d} = J_0(\kappa|x|) + 2\sum_{n=1}^{\infty} i^n J_n(\kappa|x|)\cos(n\beta), \tag{4.2}$$

where in this case β is the angle between x and d. Thus, writing $d_j = \left(\cos(\gamma_j), \sin(\gamma_j)\right)$ each basis function is written in polar coordinates as

$$\phi_j(r,\theta) := J_0(\kappa r) + 2\sum_{n=1}^{\infty} i^n J_n(\kappa r)\left(\cos(n\theta)\cos(n\gamma_j) + \sin(n\theta)\sin(n\gamma_j)\right).$$

and defining,

$$c_n = \begin{cases} J_{0,\kappa}^* & n = 0 \\ 2i^n J_{n,\kappa}^* & n > 0, \end{cases} \tag{4.3}$$

we get an expansion similar to (3.3) and then, we follow the $MFS-QR$ approach step by step.

The algorithm that we proposed in this paper is able to improve the conditioning in some simple situations. It would be interesting to investigate if it could be applied to improve other Trefftz-type methods, which typically lead to ill-conditioned matrices. For example, in [15], the authors studied the p-version of the plane wave discontinuous Galerkin method (PWDG). In that case, the domain Ω is discretized in a finite element partition and for each of the elements, the numerical approximation is given by a linear combination of p plane waves, as in (4.1). The PWDG is a powerful method that is efficient even in a much more general context than that was considered in this paper. For example, it is effective for complicated domains or more general models with piecewise constant wave numbers. However, as was pointed out in that reference, for high-dimensional local bases, it has been observed that PWDG

approaches suffer from serious ill-conditioning and without an appropriate preconditioning (e.g., [18]) or a good choice of the bases, it is impossible to obtain meaningful results for large p. Instead of the local expansion in terms of plane waves, we wonder if expanding in terms of the new base functions of the *PWM-QR*, which spans the same functional space as the plane waves, could improve the conditioning allowing to consider larger choices of p. The main difficulty in that case, probably, would be the fact that we will not have a closed form for computing the oscillatory integrals needed to build the matrix, and would need to use expensive numerical quadratures.

5 Numerical results

Next, we illustrate the performance of the *MFS-QR* and *PWM-QR* through some numerical examples. We will show results for the error in the L^2 norm on the boundary which was estimated by a quadrature rule involving 10,000 points $z_i \in \partial\Omega$. We will also present some results for the condition number which was calculated as the quotient between the largest and smallest singular values of the matrices of the systems (2.4) or (3.8) and similar systems for the plane waves method. In some cases, we will also present some numerical results obtained with the *Direct-MFS* and *Direct-PWM*. In these cases, the least-squares problems for calculating the coefficients of the linear combination were solved by using Matlab command *linsolve*, which uses QR factorization with column pivoting. We will observe that the results obtained with the *MFS-QR* and *PWM-QR* are much better, which shows that the algorithm proposed in this paper is better than just computing the QR decomposition of the MFS/PWM stiffness matrices, assembled with the usual bases in a standard way.

5.1 Unit disk

The first example was already considered in [7]. The domain Ω is the unitary disk and the solution of the boundary value problem is given by

$$u(x) = -\frac{1}{4} Y_0(\kappa|x-\rho|), \ x \in \bar{\Omega},$$

where $\rho = (x_0, 0)$, for some $x_0 > 1$ and we took $\kappa = 8$.

The first row of plots of Fig. 1 shows the errors (left plot) and the condition number (right plot), as a function of N, obtained when applying the *Direct-MFS*, the *MFS-QR*, the *Direct-PWM*, and the *PWM-QR*, for $R = 1.5$ and $x_0 = 3$.

The left plot shows that the *Direct-MFS* and the *MFS-QR* present similar results and allow to reach the machine precision, for $N > N_0 \approx 90$. However, the condition number associated with *Direct-MFS* grows exponentially while for the *MFS-QR*, the condition number is very small and almost constant, independently of N. The *Direct-PWM* and *PWM-QR* allow to obtain similar results for $N < N_1 \approx 60$ and in this case the convergence is faster than that was obtained with the MFS. For $N > N_1$, the *PWM-QR* is superior due to the high ill-conditioning of the *Direct-PWM*. In Fig. 2 (left), we plot the l^∞ norm of the vectors $\boldsymbol{\alpha}^{Direct-MFS}$, $\boldsymbol{\alpha}^{MFS-QR}$, $\boldsymbol{\alpha}^{Direct-PWM}$, and $\boldsymbol{\alpha}^{PWM-QR}$ (as a function of N) which are smaller than one in all the cases.

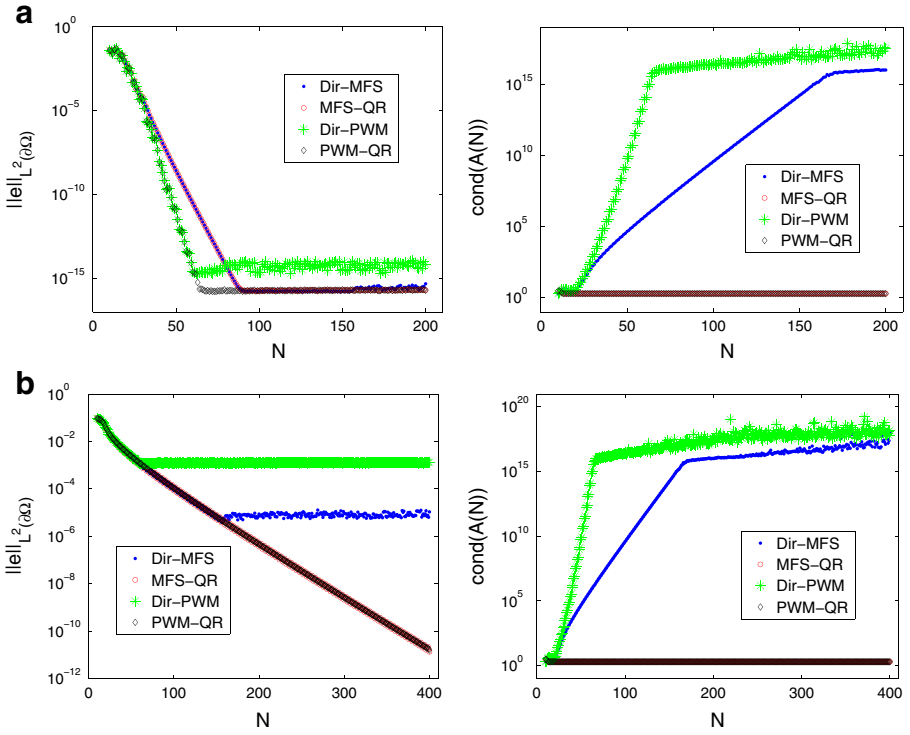

Fig. 1 Plot of the errors (left plot) and the condition number (right plot), as a function of N for the *Direct-MFS*, *MFS-QR*, *Direct-PWM*, and *PWM-QR* for **a** $x_0 = 3 > R = 1.5$ and **b** $x_0 = 1.1 < R = 1.5$

Next, we consider $x_0 = 1.1$ for which $x_0 < R$. In the second row of plots of Fig. 1, we show the error and condition number for this choice of x_0. In this case, the *Direct-MFS* and *MFS-QR* provide the same accuracy for $N < N_0 \approx 160$ and the same happens for the *Direct-PWM* and *PWM-QR*, but now for $N < N_1 \approx 60$.

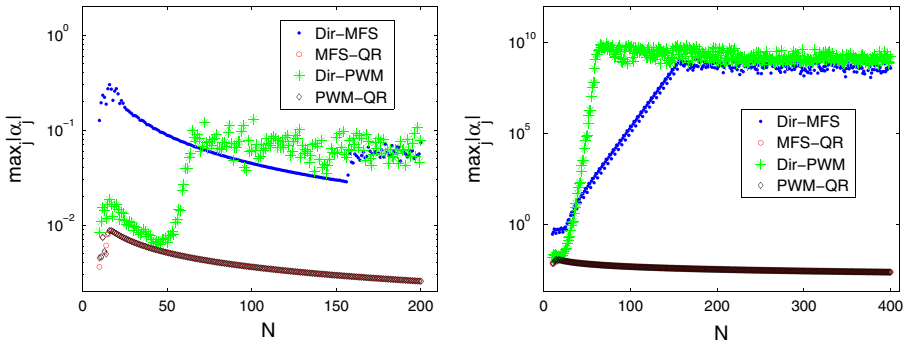

Fig. 2 Plot of the l^∞ norm of the vector of coefficients in the *Direct-MFS*, *MFS-QR*, *Direct-PWM*, and *PWM-QR*, for $x_0 = 3 > R = 1.5$ (left plot) and $x_0 = 1.1 < R = 1.5$ (right plot)

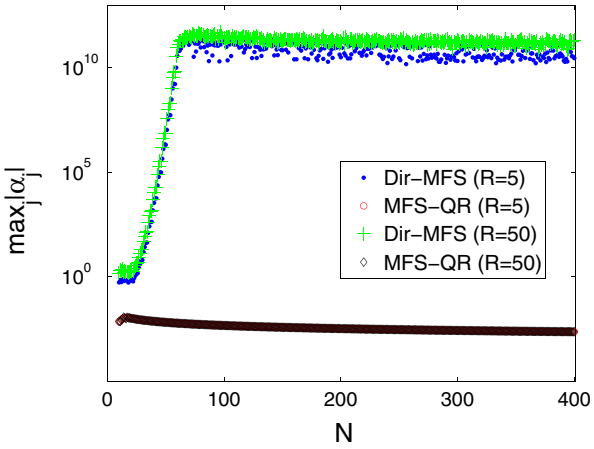

Fig. 3 Plot of the l^{∞} norm of the vector of coefficients in the *Direct-MFS* and *MFS-QR*, for $x_0 = 1.1$, when $R = 5$ and $R = 50$

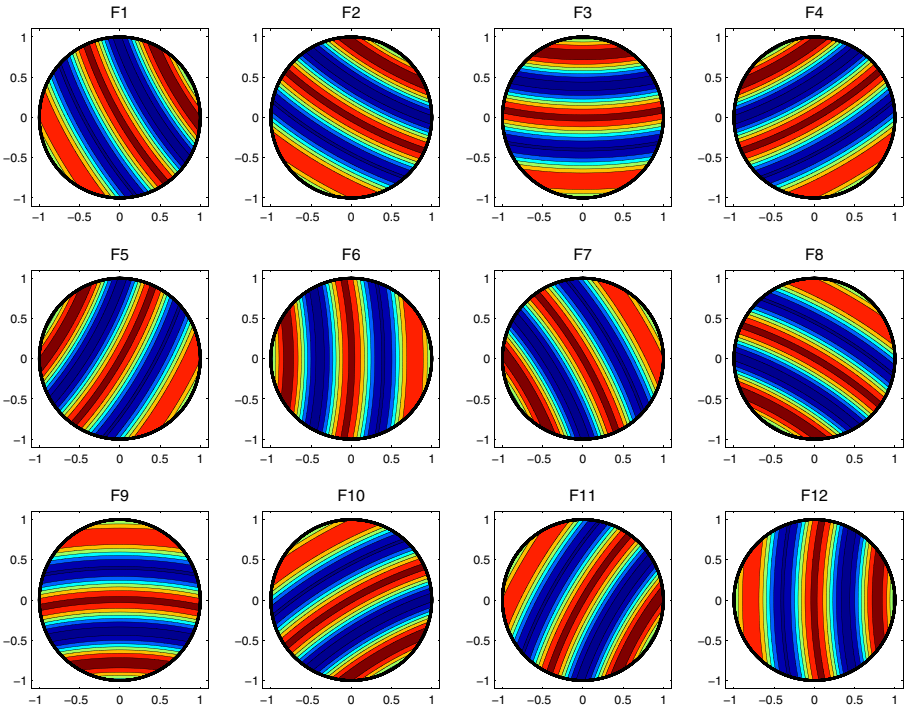

Fig. 4 Plots of the restrictions of the basis functions for the *Direct-MFS* to the unit disc, when $N = 12$ and $\kappa = 8$

However, for $N > N_0$ (resp. $N > N_1$), the convergence of the *Direct-MFS* (resp. *Direct-PWM*) breaks down due to ill-conditioning, while the *MFS-QR* (resp. *PWM-QR*) presents a smooth convergence curve and again very small condition number, independently of N.

As discussed in [7], in this case, the auxiliary curve where we place the source points encloses a singularity of the analytic continuation of the solution u and the norm of the vector of coefficients shall grow exponentially. This result is illustrated in Fig. 2 (right). The coefficients of the *Direct-PWM* also grow exponentially. On the other hand, the coefficients of the *MFS-QR* and of the *PWM-QR* do not grow and are always smaller than one.

The difference of the performances of the *Direct-MFS* and the *MFS-QR* is even more evident if we increase the parameter R, which means to place the source points on a larger circumference. If we take $R = 5$ or $R = 50$, the convergence of *Direct-MFS* stagnates at a value of order 10^{-3}, while the *MFS-QR* presents a smooth convergence curve and allows to reach the machine precision, keeping a very small condition number. Again, the norm of the vector of the *Direct-MFS* coefficients grows exponentially but for the *MFS-QR*, all the coefficients are smaller than one, independently of N, as illustrated in Fig. 3.

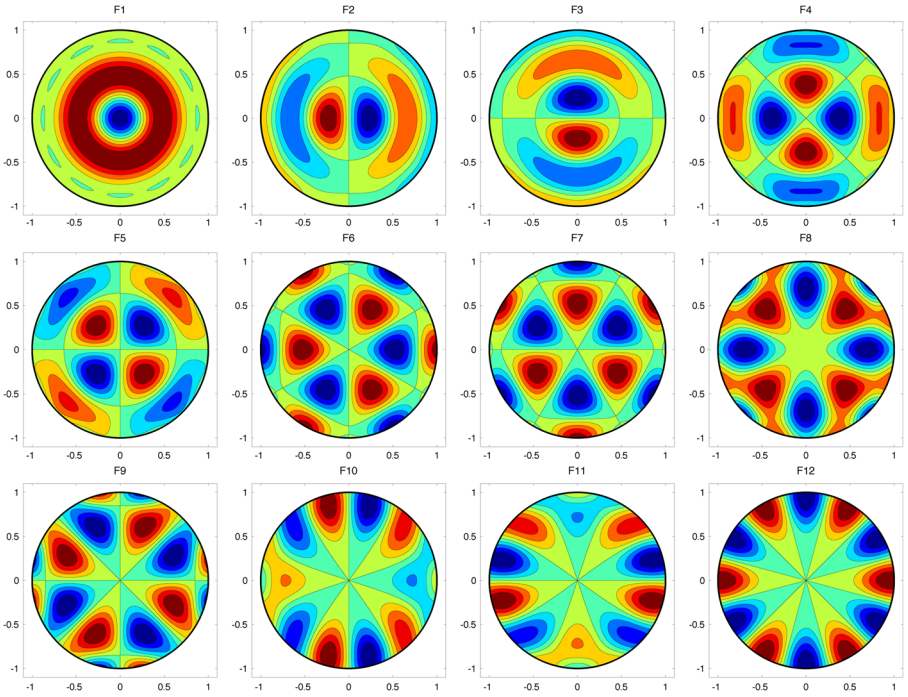

Fig. 5 Plots the basis functions associated with the *MFS-QR* that spans the same functional space as the functions plotted in Fig. 4, but are much more better conditioned

The idea of the *MFS-QR* is to perform a change of basis to the classical MFS. The new functions span the same space as the original method, but are much better conditioned. Next, we will show the plots of the new basis functions. We considered $N = 12$ source points placed on a circumference of radius $R = 5$. In Fig. 4, we plot the restrictions of the basis functions for the *Direct-MFS* to the unit disc, when $\kappa = 8$. In Fig. 5, we plot the new basis functions associated with the *MFS-QR* that spans the same functional space as the previous functions, but are much more better conditioned.

In Fig. 6, we plot similar results for the *MFS-QR*, but for a higher frequency $\kappa = 30$.

Next, we consider the case where the exact solution of the boundary value problem is given (in polar coordinates) by $u(r, \theta) = e^{im\theta} J_m(\kappa r)/J_m(\kappa)$, for $m \in \mathbb{N}$. In the first case, we fix $m = 2$. Figure 7 shows the convergence curve for $\kappa = 1, 10, 100$ (left plot) and $\kappa = 1000$ (right plot). We can obtain errors close to machine precision, but larger values of κ require to use a larger number of source points, N.

In the last simulation with circular domains, we fix $\kappa = 1$ and consider the parameters $m = 10, 50, 90, 130$. Figure 8 shows the convergence curve (left plot) and l^∞ norm of the vector of coefficients of the *MFS-QR* (right plot). Again, we can obtain

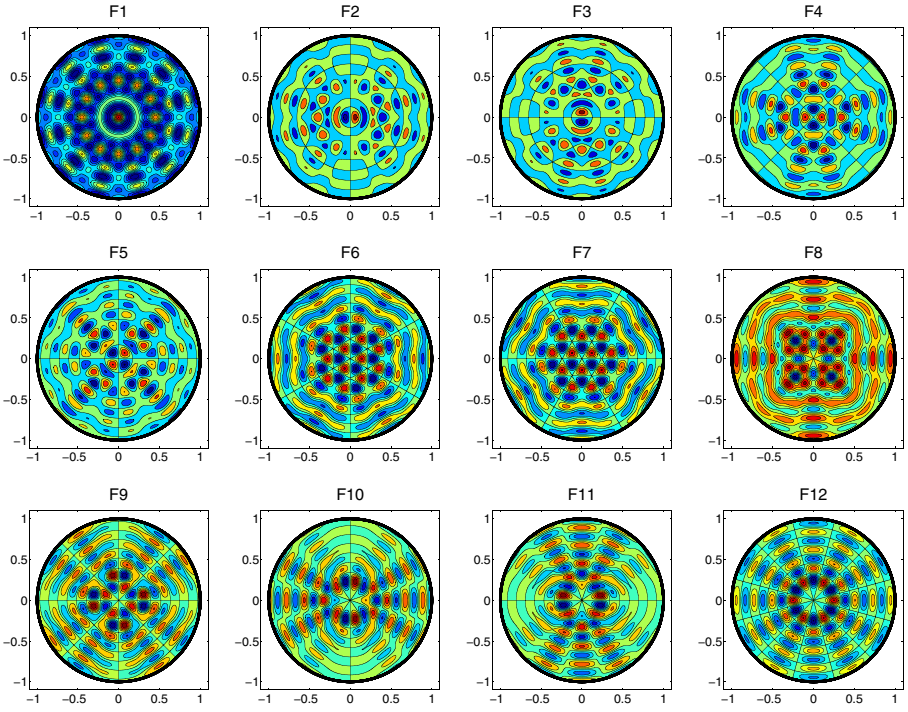

Fig. 6 Plots the basis functions associated with the *MFS-QR*, for $N = 12$ and $\kappa = 30$

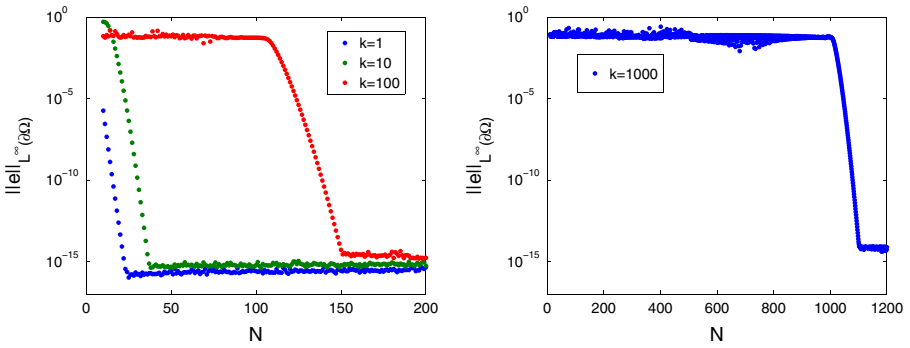

Fig. 7 Convergence curve of the *MFS-QR* for $\kappa = 1, 10, 100$ (left plot) and $\kappa = 1000$ (right plot), when the exact solution is given by $u(r,\theta) = e^{i2\theta} J_2(\kappa r)/J_2(\kappa)$

errors close to machine precision, for sufficiently large number of source points. The coefficients of the *MFS-QR* linear combination are always smaller than one.

5.2 Elliptical domains

In this section, we will show some numerical results obtained for elliptical domains, whose boundary is parameterized by

$$\{(2\cos(\theta), \sin(\theta)),\ 0 \leq \theta < 2\pi\} \tag{5.1}$$

for some $a > 0$.

The first example was considered in [4]. We define $a = 2$ and the boundary data is given by $g(x, y) = e^{i(x^2+y^2)} \sin(x + y)$. As in [4], the source points for the MFS were taken for $R = 50$. Figure 9 shows results for the error and condition number of the four numerical approaches considered in this paper.

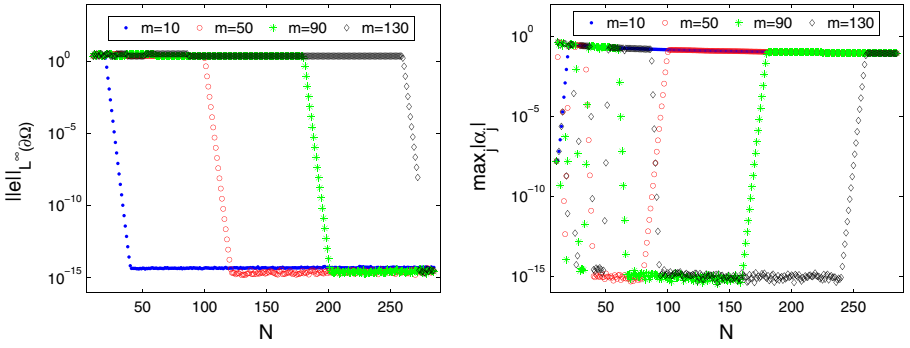

Fig. 8 Convergence curve (left plot) and l^∞ norm of the vector of coefficients of the *MFS-QR* (right plot) for $\kappa = 1$ and $m = 10, 50, 90, 130$. In each case, the exact solution is given by $u(r,\theta) = e^{im\theta} J_m(r)/J_m(1)$

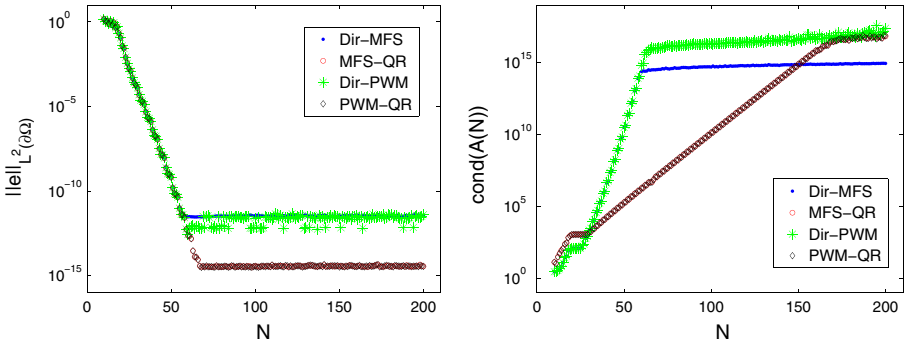

Fig. 9 Plot of the errors (left plot) and the condition number (right plot), as a function of N for the *Direct-MFS*, *MFS-QR*, *Direct-PWM*, and *PWM-QR* for an elliptical domain

In this case, the MFS and the PWM present similar results, as expected, since the source points are located in a *large* circumference. However, as was also observed in [4], the convergence of the *Direct-MFS* and *Direct-PWM* stagnates at a value of order 10^{-11}, while the *MFS-QR* and *PWM-QR* proposed in this paper allow to exhaust the machine precision level for $N > N_0 \approx 60$.

Next, we show some numerical results for ellipses with growing eccentricity. In Fig. 10, we plot the convergence curve (left plot) and the condition number (right plot) for $a = 2, 3, 4, 5, 6, 7$, obtained with the *MFS-QR*. We observe that for very elongated ellipses, the results were not so good. For example, for $a = 7$, we are not able to improve an error of order 10^{-2}. In this case, placing the source points on a circumference, as we consider in this paper, is not a good strategy (e.g., [2, 7]) and we should consider a different curve, like an elongated ellipse containing $\bar{\Omega}$.

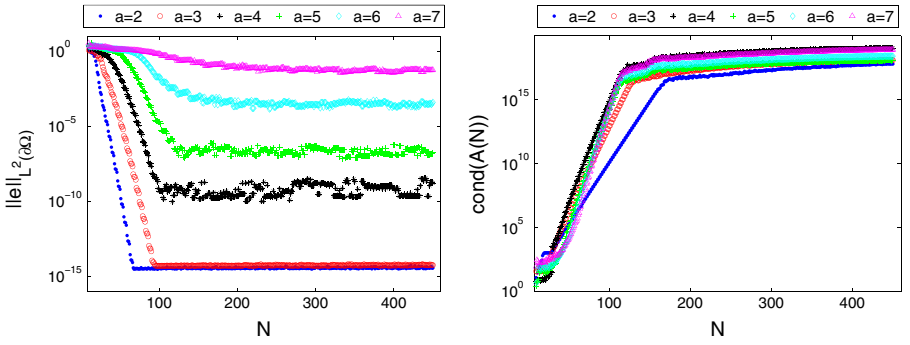

Fig. 10 Convergence curve (left plot) and the condition number (right plot), for elliptical domains with $a = 2, 3, 4, 5, 6, 7$, as a function of N

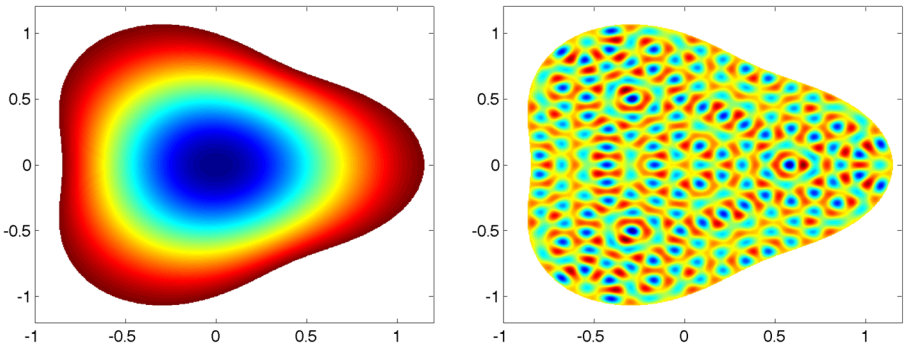

Fig. 11 Plots of the solutions of the boundary value problem for $\kappa = 3$ (left plot) and $\kappa = 50$ (right plot)

5.3 General smooth domain: smooth boundary data

In this example, we considered the application of the *Direct-MFS*, *MFS-QR*, *Direct-PWM*, and *PWM-QR* in an example with the domain whose boundary is defined though

$$\left\{(1 + \frac{3}{20}\cos(3\theta))(\cos(\theta), \sin(\theta)),\ 0 \leq \theta < 2\pi\right\} \tag{5.2}$$

and the boundary data is given by $g(x, y) = 1$. We considered simulations with two different frequencies ($\kappa = 3$ and $\kappa = 50$) and obtained the following results for the L^2 norm of the error on the boundary, when applying the *PWM-QR* with $N = 300$:

$$\|e\|_{L^2(\partial\Omega)} = 2.4 \times 10^{-13},\ \text{for } \kappa = 3$$

and

$$\|e\|_{L^2(\partial\Omega)} = 2.13 \times 10^{-7},\ \text{for } \kappa = 50.$$

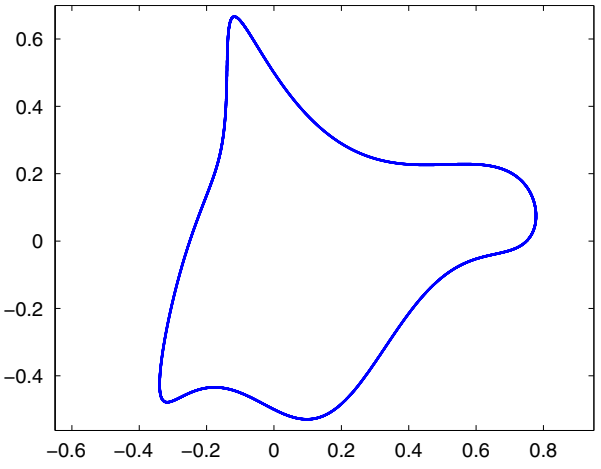

Fig. 12 Plot a domain parametrized by (5.3)

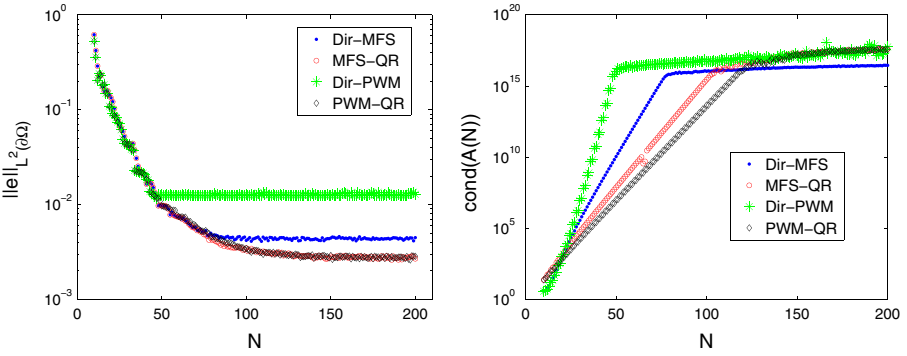

Fig. 13 Plot of the errors (left plot) and the condition number (right plot), as a function of N for the *Direct-MFS*, *MFS-QR*, *Direct-PWM*, and *PWM-QR* in an example with non-smooth boundary data

Similar results were obtained with the *MFS-QR*. In Fig. 11, we plot the solutions of the boundary value problem for $\kappa = 3$ and $\kappa = 50$.

5.4 General smooth domain: non-smooth boundary data

The last example was also considered in [4]. The boundary of the domain is parametrized by

$$\left\{\frac{1}{4}\left(\cos(\theta)\left(2+\cos(\theta)+\frac{1}{2}\sin(2\theta)\right),\ \sin(\theta)\left(2-\cos(\theta)+\frac{\sin(4\theta)}{2}\right)\right),\ 0\le\theta<2\pi\right\} \tag{5.3}$$

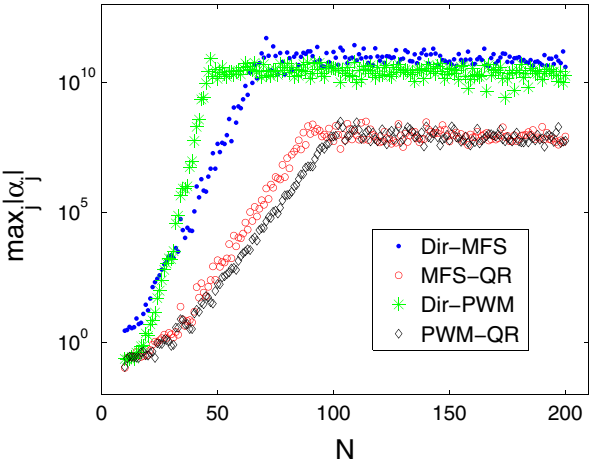

Fig. 14 Plot of the l^∞ norm of the vector of coefficients in the *Direct-MFS*, *MFS-QR*, *Direct-PWM*, and *PWM-QR*, for an example with non-smooth boundary data

which is plotted in Fig. 12. The boundary data is non-smooth and given by $g(x, y) = |\sin(x) + y|$ and we took $\kappa = 8$ and $R = 1$.

Figure 13 shows results obtained with the *Direct-MFS*, *MFS-QR*, *Direct-PWM*, and *PWM-QR*. In this case, the results are not so good, which was expected since the boundary data are non-smooth. However, even in this case, the *MFS-QR* and *PWM-QR* are superior to the *Direct-MFS* and *Direct-PWM*. The magnitude of the coefficients of the linear combinations are plotted in Fig. 14.

6 Conclusions

We proposed an algorithm for performing a change of basis in the method of fundamental solutions and the plane waves method. This allows to obtain a new set of basis functions that span exactly the same functional space of the original meshless method, but is much better conditioned. For the particular case of circular domains, the new algorithm allows to reach the machine precision, keeping the condition number of order $O(1)$, independently of the number of basis functions.

Acknowledgements I would like to thank the anonymous referees for many suggestions that clearly improved the paper.

References

1. Alves, C.J.S.: On the choice of source points in the method of fundamental solutions. Eng. Anal. Bound. Elem. **33**, 1348–1361 (2009)
2. Alves, C.J.S., Antunes, P.R.S.: The method of fundamental solutions applied to the calculation of eigenfrequencies and eigenmodes of 2D simply connected shapes. Comput. Mater. Continua **2**, 251–266 (2005)
3. Alves, C.J.S., Antunes, P.R.S.: The method of fundamental solutions applied to some inverse eigenproblems. SIAM J. Sci. Comp. **35**, A1689–A1708 (2013)
4. Alves, C.J.S., Valtchev, S.S.: Numerical comparison of two meshfree methods for acoustic wave scattering. Eng. Anal. Bound. Elements **29**, 371–382 (2005)
5. Antunes, P.R.S.: Reducing the ill conditioning in the method of fundamental solutions, submitted
6. Babŭska, I., Melenk, J.M.: The partition of unity method. Internat J. Numer. Methods Eng. **40**, 727–758 (1997)
7. Barnett, A.H., Betcke, T.: Stability and convergence of the method of fundamental solutions for Helmholtz problems on analytic domains. J. Comput. Phys. **227**(14), 7003–26 (2008)
8. Bogomolny, A.: Fundamental solutions method for elliptic boundary value problems. SIAM J. Numer. Anal. **22**(4), 644–669 (1985)
9. Borzdov, G.N.: Plane-wave superpositions defined by orthonormal scalar functions on two and three dimensional manifolds. Phys. Rev. E **61**, 4462–78 (1999)
10. Cessenat, O., Despres, B.: Application of an ultra weak variational formulation of elliptic PDEs to the two-dimensional Helmholtz problem. SIAM J. Numer. Anal. **35**, 255–299 (1998)
11. Colton, D., Kress, R.: Inverse Acoustic and Electromagnetic Scattering, 3rd Edn. Springer, Berlin (2013)
12. Fairweather, G., Karageorghis, A.: The method of fundamental solutions for elliptic boundary value problems. Adv. Comput. Math. **9**, 69–95 (1998)
13. Fornberg, B., Piret, C.: A stable algorithm for flat radial basis functions on a sphere. SIAM J. Sci. Comput. **30**(1), 60–80 (2007)

14. Gittelson, C.J., Hiptmair, R., Perugia, I.: Plane wave discontinuous Galerkin methods: analysis of the h-version. ESAIM M2AN **43**, 297–331 (2009)
15. Hiptmair, R., Moiola, A., Perugia, I.: Plane wave discontinuous Galerkin methods for the 2D Helmholtz equation: analysis of the p-version. SIAM J. Numer. Anal. **49**, 264–284 (2011)
16. Hon, Y.C., Li, M.: A discrepancy principle for the source points location in using the MFS for solving the BHCP. Int. J. Comput. Methods **6**, 181–197 (2009)
17. Hu, Q., Yuan, L.: A weighted variational formulation based on plane wave basis for discretization of Helmholtz equations. Int. J. Numer. Anal. Model. **11**, 587–607 (2014)
18. Hu, Q., Zhang, H.: Substructuring preconditioners for the systems arising from plane wave discretizations of Helmholtz equations. SIAM J. Sci. Comput. **38**(4), 2232–2261 (2016)
19. Katsurada, M.: A mathematical study of the charge simulation method. II. J. Fac. Sci. Univ. Tokyo Sect. IA Math. **36**(1), 135–162 (1989)
20. Katsurada, M.: Charge simulation method using exterior mapping functions. Jpn. J. Ind. Appl. Math. **11**(1), 47–61 (1994)
21. Kitagawa, T.: On the numerical stability of the method of fundamental solution applied to the Dirichlet problem. Jpn. J. Appl. Math. **5**, 123–33 (1988)
22. Kupradze, V.D., Aleksidze, M.A.: The method of functional equations for the approximate solution of certain boundary value problems. U.S.S.R Comput. Math. Math. Phys. **4**, 82–126 (1964)
23. Kuttler, J.R., Sigillito, V.G.: Bounding eigenvalues of elliptic operators. SIAM J. Math. Anal. **9**(4), 768–773 (1978)
24. Mathon, R., Johnston, R.L.: The approximate solution of elliptic boundary-value problems by fundamental solutions. SIAM J. Numer. Anal. **14**, 638–50 (1977)
25. Monk, P., Wang, D.: A least-squares method for the Helmholtz equation. Comput. Methods Appl. Mech. Eng. **175**, 121–136 (1999)
26. Olver, F.W.J.: Bessel functions of integer order. In: Abramowitz, M., Stegun, I.A. (eds.) Handbook of Mathematical Functions with Formulas, Graphs, and Mathematical Tables. Dover, New York (1972)
27. Schaback, R.: Error estimates and condition numbers for radial basis function interpolation. Adv. Comput. Math. **3**, 251–64 (1995)